Rare Metal Materials and Engineering
Volume 55, Issue 10, October 2026
Available online at www.rmme.ac.cn

Science Press

Cite this article as: Liu Hongbo, Li Aojie, Ma Wenjiang, et al. Molecular Dynamics Simulations of Aluminum-Based Core-Shell Nanocomposite with Carbon Coating Under Linear Injection of Heat Energy[J]. Rare Metal Materials and Engineering, 2026, 55(10): 2442-2449. DOI: https://doi.org/10.12442/j.issn.1002-185X.20250491.

ARTICLE

Molecular Dynamics Simulations of Aluminum-Based Core-Shell Nanocomposite with Carbon Coating Under Linear Injection of Heat Energy

Liu Hongbo[1], Li Aojie[2], Ma Wenjiang[3], Chen Zhanghua[1], Liu Yi[2]

[1] School of Mathematics and Physics, University of Science and Technology Beijing, Beijing 100083, China; [2] Faculty of Civil Engineering and Mechanics, Kunming University of Science and Technology, Kunming 650031, China; [3] Basic Experimental Center for Natural Science, University of Science and Technology Beijing, Beijing 100083, China

Abstract: A novel core-shell nanocomposite was prepared by coating carbon onto aluminum nanoparticles (ANPs). As a typical energetic material, this nanocomposite absorbs the heat energy prior to ignition and combustion. Molecular dynamics simulations were used to elucidate the phase-transition mechanism of the nanocomposite upon heating and to analyze migration at the core-shell boundary. The results show that the critical melting point of carbon-coated ANPs (8 nm in diameter), at which the material transitions from solid to liquid, is approximately 1050 K. The interatomic potential energy of nanocomposites is lower than that of aluminum cores. Therefore, upon injection of thermal energy, the initial amorphous phase transforms into the liquid phase, which then diffuses from the surface to the core. Low interatomic potential energy leads to an earlier transition to the liquid phase. Furthermore, the core-shell ratio is the main factor affecting the critical melting point. The higher the core-shell ratio, that is, the thinner the carbon coating, the lower the melting point. Therefore, effectively controlling this parameter is an important indicator of ignition efficiency.

Key words: molecular dynamics; carbon coating; ANP; core-shell nanocomposite

1 Introduction

With advances in aerospace dynamics, many researchers have discovered, tested, and characterized the chemical composition of propellants. Aluminum nanoparticles (ANPs) are common metal additives, and their applications in solid propellants, including composite, fuel-rich, and composite-modified double-base propellants, have received significant attention[1]. This is because ANPs can effectively reduce the production of toxic gases and increase combustion efficiency to 54% without any negative effect on performance[2]. With a large specific surface area, ANPs cause more pronounced positive changes than micro-sized particles[3]. However, high energy density, high reactivity, and a large specific surface area also pose issues such as agglomeration[4] and surface oxidation. It is reported that the aluminum oxide shell of ANPs does not break or shatter but deforms during the oxidation process[5]. The extent of shell deformation is determined by the particle diameter. Besides, an oxidation kinetics study[6] has revealed that the growth of γ -Al_2O_3 crystallites and their diffusion to the surface and grain boundaries accelerate the oxidation rate. It has also been found that anions are transported through an amorphous layer and an underlying nanocrystalline oxide layer[7]. The oxidation kinetics of aluminum are highly related to the oxygen concentration, so the addition of a non-oxidizing gas can increase the critical oxidation temperature of aluminum powder[8].

In gas environments, surface passivation of ANPs is a reasonable approach for inhibiting oxidation. The surface passivation of ANPs has been widely studied using advanced experimental characterization[9–10] or numerical simulations[11–13]. Apart from the investigated coating applications involving organic molecules or metals[14], carbon

Received date: October 24, 2025
Foundation item: National Natural Science Foundation of China (92160201)
Corresponding author: Chen Zhanghua, Ph. D., Professor, University of Science and Technology Beijing, Beijing 100083, P. R. China, E-mail: chenzhanghua@ustb.edu.cn

is another potential coating material for the surface passivation of ANPs. Importantly, according to the Lindemann criterion, the atoms in the amorphous structure of the carbon coating are highly disordered, and this structure is prone to disintegration before the crystallization of the aluminum phase[15–16]. It has been reported that carbon-based graphene, a novel 2-dimensional material, has extensive applications due to its excellent corrosion resistance[17]. ANPs should be surface-protected before encapsulation with spherical carbon to form a core-shell nanocomposite. This core-shell structure creates distinct environments for atoms, reaching Lindemann's vibrational displacement threshold at different interface temperatures, thereby enabling control over the initial sequence of melting. This type of composite is prepared using spark plasma sintering and exhibits higher Vickers hardness and thermal conductivity than bulk aluminum[18]. High-energy ball milling is also feasible for producing carbon-aluminum composites, and the resulting composites exhibit high thermal conductivity and a low thermal expansion coefficient[19]. Furthermore, the carbon coating can even overcome certain intrinsic shortcomings of liquid metals[20].

As metal propellants, ANPs undergo two main stages in the combustion process: energy-injection and heat release[21]. In particular, the energy-injection or heating stage of ANPs is critical to overall development because ANP breaking and melting govern the diffusion of oxygen atoms. This mechanism has been uncovered in multiple recent studies. It is well established that nanoparticle size significantly affects the melting point, which decreases as nanoparticle size decreases[22–24]. Besides, surface pre-melting and heterogeneous nucleation at interfaces are particularly pronounced in core-shell systems, where confinement alters thermal transport pathways[25–26]. However, the internal changes and behavior of graphene-coated ANP nanocomposites during linear heating remain poorly understood. Firstly, the ANP with over 850 aluminum atoms exhibits an obvious transition from the solid to the liquid phase[27].

Nevertheless, the solid-liquid phase stability of carbon-coated ANPs remains to be further investigated, as it is closely related to the melting point of the nanocomposites. Secondly, it is shown that increasing the critical point and the fusion heat imposes a compressive force on the ANP core[28]. In core-shell systems, the boundary between the core and the shell may change the loading effect of the carbon coating on the aluminum core. Thirdly, the application of the ReaxFF force field has demonstrated the feasibility and advantages of non-fixed interatomic potentials[29]. In future work, this approach will be used to simulate reaction mechanisms at the atomic level[30–31]. It is worthwhile to perform molecular dynamics (MD) simulations of carbon as well, given the presence of different atom types.

Due to space limitations, the present study mainly focuses on changes in the core-shell structure and its boundary. To ensure precise and reliable results, MD simulations were used to elucidate the atomic-scale phase-transition stages of ANPs and the coating. The modeling and point-to-point analysis of the core-shell boundary between aluminum and carbon demonstrate the innovativeness of the present study.

2 Materials and Methods

2.1 Molecular dynamics simulations

An uncoated ANP with a diameter of 8 nm contains only about 1.6×10^6 aluminum atoms in the model[32]. Its nano-diameter inhibits the coating-core interaction while amplifying the surface effect. At the atomic scale, MD simulation is a powerful tool for investigating thermal dynamics and structural parameters of alloys and nanocomposites, such as titanium alloys[33–34] and even organic-matter-coated ANPs[13, 35]. By solving the equations of motion for atoms using classical mechanics, MD simulations provide a step-by-step understanding of aluminum and carbon atoms in carbon-coated ANPs. In the present study, an open-access classical MD program, LAMMPS[36] (Version: 64-bit-28Mar2023), was used to simulate all carbon-coated models under various conditions. LAMMPS uses the Velocity-Verlet algorithm, which produces convincing dynamic results to obtain all atomic trajectories. In addition, an interatomic force field can be used to compute the attractive and repulsive interactions between pairs of atoms or clusters. The Tersoff-type force field applied in the present study was developed by Plummer et al[37–38]. The potential for carbon-aluminum interactions was verified. Comprehensive benchmark tests, based on experimental measurements and density functional theory simulations, were conducted to confirm the model's reliability in this study.

2.2 Computational models

Because the melting point of the ANP is highly related to its radius, it is reasonable to model ANPs with the same size. As shown in Fig. 1, three models were simulated in this study. All ANP cores were modeled as nearly ideal spheres with a diameter of 8 nm. Based on the parameters of bulk aluminum, the crystal structure of ANPs was established as a typical face-centered cubic (fcc) lattice with a constant of 0.4046 nm. The core-shell ratio was defined as the ANP diameter divided by the core-shell thickness. The carbon coating was modeled with three thicknesses: 0.5, 1, and 1.5 nm. To obtain carbon-coated ANP models with low potential energy, all models were thermally relaxed at 300 – 400 K. All models were visualized using the OVITO program[39], and coordination and common-neighbor analyses were used to identify key structural trends.

2.3 Simulation parameters

ANP models with carbon coatings of different thicknesses were placed in a cubic simulation box. The simulation box has dimensions of 20 nm×20 nm×20 nm, and the planar boundaries in each direction are set to periodic boundary conditions. The simulation box is a vacuum, eliminating potential influences from other molecules or clusters.

Before heat injection, all models were optimized using the Polak-Ribière conjugate gradient algorithm to minimize

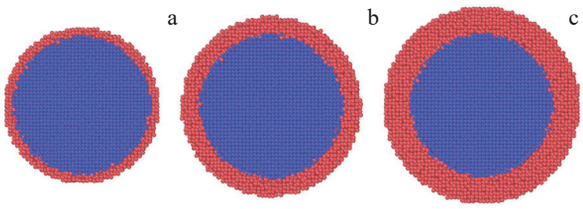

Fig.1 Cross-sections of 8 nm ANP models with carbon coatings of different thicknesses: (a) 0.5 nm, the core-shell ratio=8; (b) 1 nm, the core-shell ratio=4; (c) 1.5 nm, the core-shell ratio =2.7

energy for subsequent MD simulations. Then the Nosé -Hoover thermostatting method was applied to linearly control the model temperature in the canonical ensemble. During the heat injection, the model temperature increased from 300 K to 1300 K over 1 ns. Although the 1 ns heating process may impose dynamic constraints on achieving complete equilibrium, this threshold remains a valid comparative metric for the studied system under the same simulation conditions. The coordinates of each atom were integrated for 1×10^6 steps in total with a time step of 1 fs. To avoid fluctuations during heating, the thermal damping coefficient in the constant-temperature algorithm was set to 100 fs.

3 Results and Discussion

3.1 Phase transition process under high temperatures

To some extent, the heating process is a precursor to nanocomposite ignition. The heating of nanocomposites relies on injecting heat energy into each atom. To eliminate potential effects of heating rates or stability, the temperature-rise curve was kept linear using thermal-state algorithms. Fig. 2 shows the heating process diagram, which lacks error bars due to computational limitations. The linear heating scheme adopted ensured minimal thermal fluctuations, as evidenced by consistent trajectories across multiple simulations. According to Fig. 2, the temperature meets its initial demand. The deviation in the rate of temperature rise can be almost ignored. Initially, the aluminum core is at about 300 K, and the fcc phase remains the predominant phase even after geometry optimization. However, the carbon coating transforms into an amorphous phase at 300 K, which is attributed to the low potential energy of carbon atoms on the surface and the limitation of coating thickness. At this temperature, the interatomic binding is too weak to maintain the stability of the lattice structure. Subsequently, as temperatures rise, the entire structure of carbon-coated ANPs enters the liquid phase. At 1300 K, the boundary between the aluminum core and the carbon shell is observed. There is no heat concentration in the overall temperature distribution, which is common for carbon-coating layers with different thicknesses.

The phase transition from the fcc and amorphous phases to the liquid phase does not occur immediately but rather gradually. Fig.3 shows the change in atomic temperature from

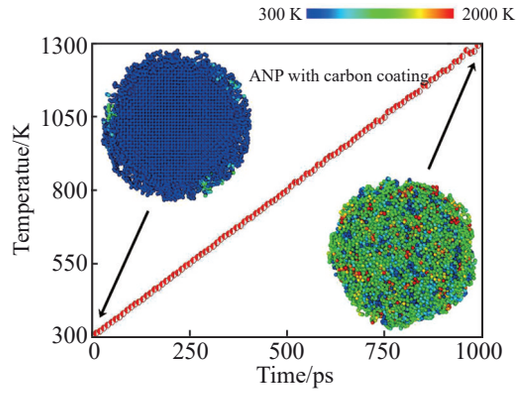

Fig.2 Linear heating process of carbon-coated ANPs from the beginning to the end

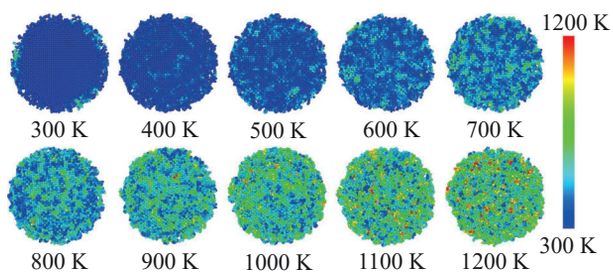

Fig.3 Phase transition state of carbon-coated ANPs at each temperature point

the beginning (300 K) to the end (1200 K). The temperatures of the aluminum core and the carbon shell are nearly equal in both directions. Neither the liquid phase nor the fcc and amorphous phases show heat concentration in the temperature distribution. Therefore, the solid core-shell boundary does not inhibit heat diffusion in the core or shell. Besides, the fcc phase in the aluminum core is reduced in the temperature range from 1000 K to 1200 K. It is inferred that the phase transition occurs mainly in this temperature range. However, the snapshot of core-shell particles at 1100 K in Fig. 3 shows no heat concentration in the distribution of the atomic temperature. It indicates that the phase transition of this core-shell nanocomposite occurs upon the injection of heat or kinetic energy, with no effect on the temperature distribution. Furthermore, this temperature-phase relationship remains unchanged before and after the transition from the fcc and amorphous phases to the liquid phase.

Compared with atomic-scale temperature measurements, structural identification using OVITO more clearly reveals the atomic state of carbon-coated ANPs during the phase transition. This method is particularly applicable to visualizing the spatial and temporal evolution of the phase transition process in real time. As shown in Fig. 4, the fcc phase of the aluminum core is surrounded by the amorphous phase of the carbon coating layer. Due to internal stress in the carbon coating, several crystalline defects are observed in the aluminum core zone. As the overall temperature rises from

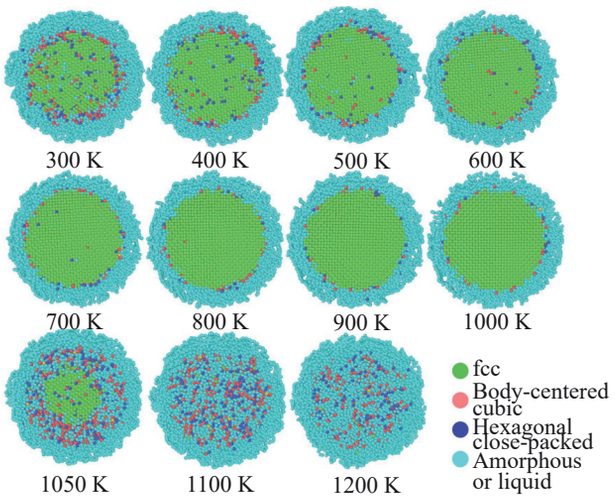

Fig.4 Phase transition state of carbon-coated ANPs at each temperature point

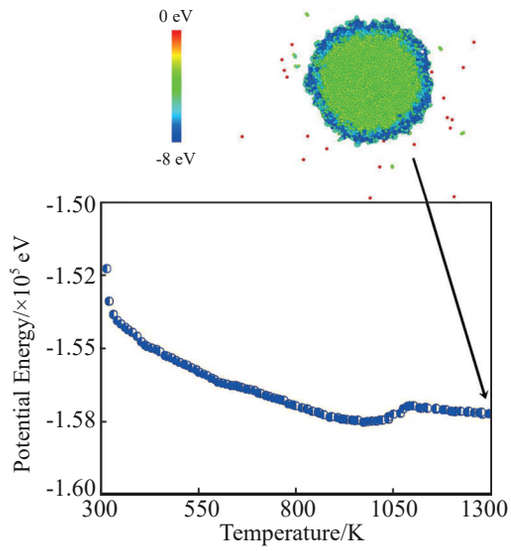

Fig.5 Change in total potential energy from 300 K to 1300 K and the atomic potential energy distribution at 1300 K

300 K to 400, 500, and 600 K, aluminum atoms gain more kinetic energy, allowing them to release internal stress. To some extent, the crystalline structure is optimized before the melting point is reached.

According to the snapshot at 1050 K, the phase transition point of carbon-coated ANPs is around 1050 K. From a structural perspective, this transformation is characterized by a shift of the phase transition boundary towards the core, i.e., from the nanoparticle surface to the core. This melting process, which begins at the surface, aligns with the Lindemann criterion. Specifically, due to the lower vibrational stability and disordered atomic arrangement of amorphous carbon coatings, they reach the critical vibrational displacement threshold earlier than the ordered crystalline aluminum core. The carbon layer undergoes a structural collapse from the amorphous phase to the liquid phase, marking the onset of the phase transition. The Lindemann parameter explains why solutes first undergo nucleation at the amorphous boundary rather than in the ordered fcc phase. As the carbon layer melts, the liquid fcc phase boundary replaces the amorphous fcc phase boundary. Under the continuous drive of thermal energy, this new boundary continues to move inward. This phase transition process persists until the lattice structure of the aluminum core is destroyed. All carbon coatings and aluminum atoms are completely transformed into the liquid phase.

In MD simulations, the magnitude of interatomic potential energy affects atomic stability and the intensity of their interactions. Changes in potential energy between atoms can trigger alterations in the state of matter. In addition, the formation of chemical bonds is closely related to the potential energy between atoms. The combination of different atoms leads to varying potential energies, and temperature changes may shift the potential energy between atoms. Fig.5 shows the change in the total potential energy of the nanocomposite from 300 K to 1300 K. Although single-trajectory data can only show thermal fluctuations, the distinct step response consistently appearing at 1050 K across multiple simulations, with noise levels indicating a phase transition, demonstrates that a phase transition occurs. The increase in temperature leads to the in-situ thermal vibration of each atom in the solid phase. During this period, the interatomic distance increases, and atomic interactions weaken. Thus, the potential energy decreases in the illustration. A step response appears at around 1050 K because in situ thermal vibration is replaced by thermal migration. According to the cross-section snapshot of the particle, atoms in the region of the carbon layer have lower potential energy than those in the aluminum core. This is why the phase transition starts at the surface and progresses to the core.

Mean-squared displacement (MSD) is an important parameter in MD simulations and measures the temporal deviation of atomic positions. Fig. 6 shows the MSD of the aluminum core and carbon shell in the nanocomposite model. Although these three trajectory curves lack error quantification, their characteristic behavior patterns are generally consistent, and all show an upward trend. The MSD curve of aluminum shows a greater upward amplitude above 1050 K, and at this point, the overall MSD curve also exhibits a larger upward slope. As shown in Fig.6, the aluminum core undergoes a phase transition at 1050 K. The climbing rate of the MSD in the liquid phase is much higher than that in the fcc solid phase, because the transition from fcc to liquid phases allows the thermal migration of aluminum atoms in a larger region than before. As kinetic energy increases, atomic diffusion intensifies. The MSD of the carbon shell shows no obvious transition throughout the simulation, confirming the differences between crystalline and non-crystalline phases. The diffusion stability of the carbon shell differs from that of the aluminum core. Besides, there is no obvious change in the

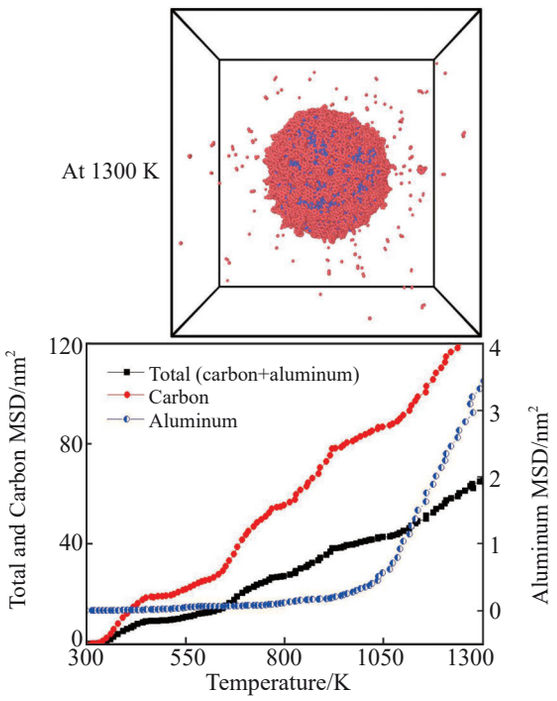

Fig.6 Change in the MSD of the core (aluminum) and the shell (carbon) in the heating process

MSD of the carbon shell before and after 1050 K. The reason is that the atomic interactions in the amorphous phase are much lower than those in the fcc phase, even though both are solid phases. With low atomic restrictions, carbon atoms are more prone to leaving their original sites. Additionally, the snapshot in Fig. 6 shows the desorption of carbon atoms or pairs during heating. As a result, the atomic restrictions are further weakened in the coating layer, and there is no critical MSD point in the carbon shell. Thus, the MSD curve of the carbon shell is more likely to be a fluctuating line.

3.2 Evaluation of the core-shell boundary before and after melting

Studies have shown that the growth of the carbon coating on the aluminum surface is primarily driven by hydrocarbon precursors and that the C-C bond remains stable during this process[40]. However, in the present study, hydrocarbon species were not used in modeling the core-shell structure. The core-shell boundary at low temperatures is not easy to expand without precursors. According to the cross-sectional snapshot in Fig. 7, the obtained core-shell boundary corresponds to a typical carbon-aluminum coupling zone, with a critical line separating carbon and aluminum. The carbon-aluminum coupling region refers to the interface between carbon and aluminum atoms. As shown in Fig.7, the microstructure of the core-shell boundary is colored by parameters. It can be seen that the initial core-shell boundary forms through simultaneous, opposite diffusion of carbon and aluminum atoms. In this process, more and more C-Al bonds are produced following the breaking of Al-Al bonds, and a clear boundary is formed between the fcc crystalline amorphous phases. It is worth noting that the core-shell boundary changes from an ideal circle to an elliptical boundary. This is due to fcc lattice anisotropy and the injection of thermal energy. Different crystal planes have different surface energies and atomic stacking densities, resulting in varying melting resistance and the formation of non-spherical, elliptical boundaries. Although the stabilized core-shell boundary exhibits a unique kinetic energy, the potential energy of the overall core-shell boundary zone still decreases, which significantly affects phase transitions within and outside the boundary zone. The structure at around 300 K confirms that the parameter state is partially stabilized.

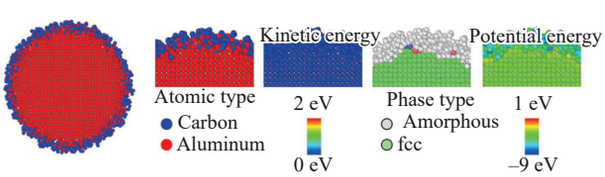

Fig.7 Different state parameters of the core-shell boundary at 300 K

Although the boundary of the core-shell structure is stabilized at room temperature, the injection of heat energy still has potential effects on the diffusion of atoms. Fig. 8 shows the distribution of carbon atoms in the core-shell boundary zone. These scatter plots are obtained from the *Y-Z* plane of the spherical model, with a cross-section thickness of 1 nm. The figure shows that injecting heat energy has little effect at temperatures below the phase transition point. During this period, kinetic energy is primarily derived from the in situ thermal vibration of atoms, which does not diffuse in the boundary zone. Above 1050 K, the source of atomic kinetic energy changes from the in-situ thermal vibration to thermal diffusion. A new diffusion mechanism, counterdiffusion, operates at the boundary. In this mechanism, carbon atoms diffuse from a high-concentration zone to a low-concentration zone, so an increasing number of atoms diffuses inward to the core. Meanwhile, aluminum atoms diffuse through the carbon coating to the surface. Consequently, the core-shell boundary widens when heat is injected above the phase transition temperature. This trend is initially observed in Fig. 7. However, due to the limited cross-sectional thickness and the extremely short time step, this change is not visible in the scatter plot.

3.3 Effects of the core-shell ratio on the heated microstructure

As discussed above, the phase transition from solid to liquid in carbon-coated ANPs begins at the outer surface of the carbon coating. In practical applications, there is no denying that nanocomposites exhibit a range of diameters[41], while the effect of coating thickness remains unclear. In this section, the core-shell ratio is redefined as the ANP radius divided by the initial coating thickness. Therefore, the core-shell ratios of ANPs with 0.5 nm-, 1.0 nm-, and 1.5 nm-thick carbon coatings are 8, 4, and 2.7, respectively.

Fig. 9 shows the change in the total energy of

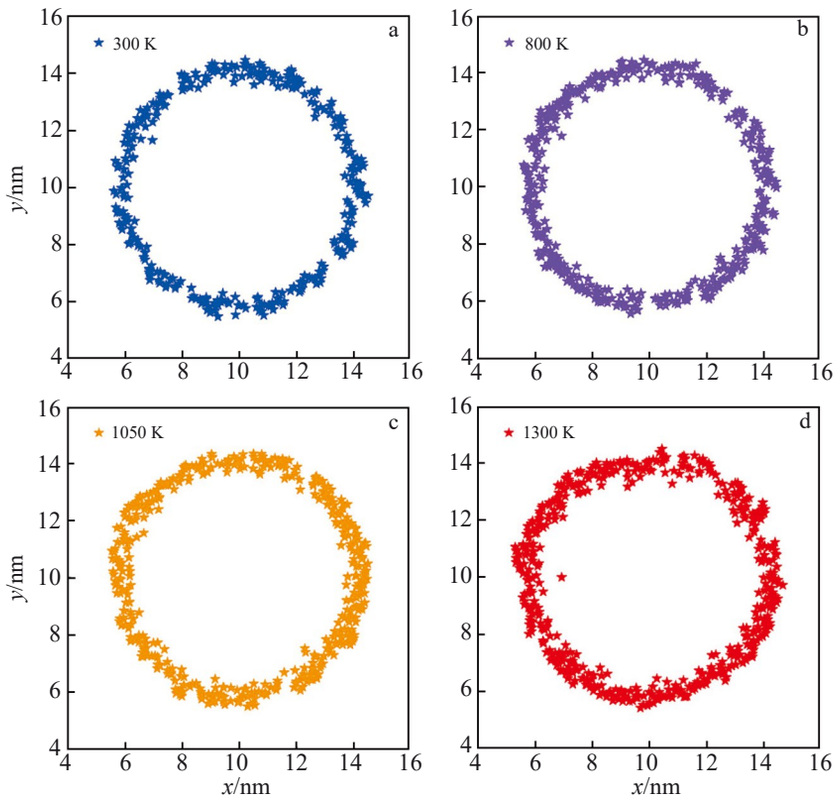

Fig.8 Atomic distributions of the core-shell boundary at 300 K (a), 800 K (b), 1050 K (c), and 1300 K (d)

nanocomposite with temperature. Because the total energy of each model is obtained by summing potential and kinetic energy, similar step responses are observed in the plots of Fig. 9. As discussed above, the frame of the step response refers to the critical phase transition point. These points for nanocomposites with core-shell ratios of 8, 4, and 2.7 are

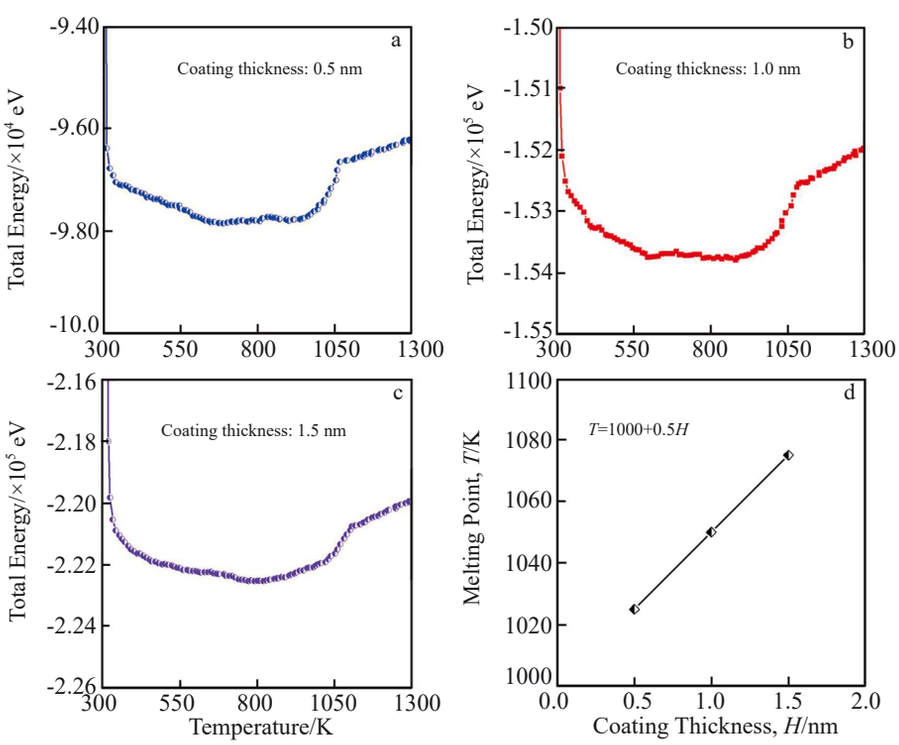

Fig.9 Plots of total energy for ANPs with carbon coating layers of different thicknesses (a–c) and their melting points (d): (a) 0.5 nm, (b) 1.0 nm, and (c) 1.5 nm

about 1025, 1050, and 1075 K, respectively. The simulation results establish a clear relationship among carbon coating, phase transition temperature, and melting time. The thinner the carbon coating, the lower the phase transition temperature. This is evidenced by the fact that ANPs with thinner carbon coatings melt earlier than those with thicker coatings. At a constant heating rate, a lower phase transition temperature results in a shorter melting time.

The mechanism underlying the effect of the core-shell ratio on the phase transition point is related to the range of the core-shell boundary. As presented in Fig. 7, the entire structure of the core-shell boundary of nanocomposites mainly includes a pure carbon coating zone and a carbon-aluminum coupling zone with a critical line separating carbon from aluminum. Because interatomic diffusion is limited at room temperature, the carbon-aluminum coupling zone does not widen as coating thickness increases. In other words, nanocomposites with a higher core-shell ratio have a relatively smaller pure carbon coating zone. To some extent, this zone can be fully substituted by the coupling zone. A coupling zone with low potential energy is prone to melting at lower temperatures. Fig. 10 compares the structures of nanocomposites with three different core-shell ratios. At 1000 K, the three nanocomposites still maintain their original state. With the rise in temperature to 1050 K, there are significantly fewer solid fcc phases in 0.5 nm-thick carbon-coated ANPs than in the other two ANPs. This is because a thin carbon coating melts earlier than a thick coating. In this process, the atomic diffusion shown in Fig.11 is also accelerated.

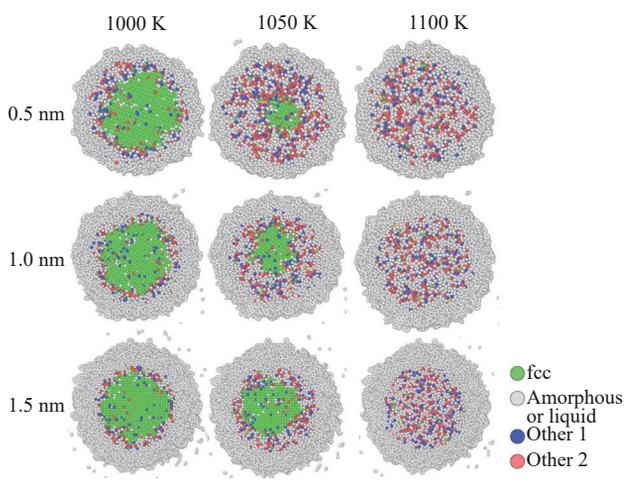

Fig.10 Cross-sections of carbon-coated ANPs during the phase transition process

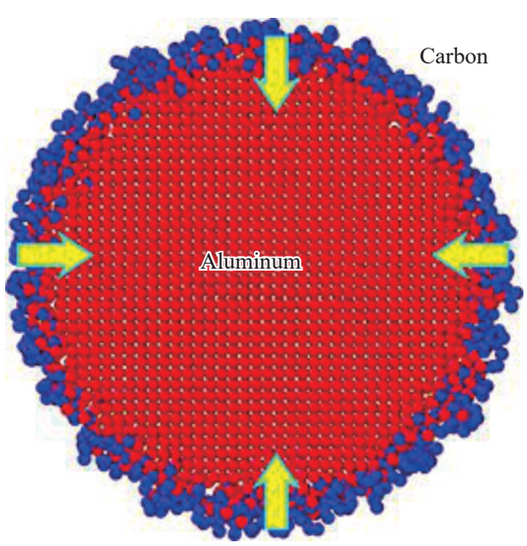

Fig.11 Schematic diagram of carbon diffusion in a nanocomposite

4 Conclusions

1) To investigate the phase transition behavior of carbon-coated ANPs and to evaluate the influence of their core-shell structure and coating boundary on metal propellant applications, MD simulations with heat injection are performed on the prepared nanocomposite.

2) The interatomic potential energy of coated nanoparticles is lower than that of bare Al cores.

3) The initial amorphous phase transitions to liquid upon heat injection, with the liquid phase diffusing from the surface toward the core.

4) Surface pre-melting is identified as a characteristic feature of the melting process in core-shell structures, initiating below the bulk melting point.

5) Increasing the core-shell ratio lowers the surface pre-melting temperature of the carbon shell.

6) For nanocomposites with an 8 nm ANP core, the melting point follows the fitted relationship T=1000+0.5H, indicating a dependence on the thickness of the pure carbon coating. Specifically, thicker carbon coatings melt later than thinner ones, which enables earlier boundary diffusion in nanocomposites with thin carbon coatings.

References

1 Pang W, Li Y, DeLuca L T *et al. Nanomaterials*[J], 2021, 11: 2749
2 Vellaisamy U, Biswas S. *Combustion and Flame*[J], 2020, 221: 326
3 Sun R, Liu P, Qi H *et al. Journal of Molecular Graphics and Modelling*[J], 2020, 100: 107667
4 DeLuca L T, Maggi F, Dossi S *et al. Chinese Journal of Explosives and Propellants*[J], 2013, 6: 1
5 Li Y, Kalia R K, Nakano A *et al. Journal of Applied Physics*[J], 2013, 114: 541
6 Korshunov A V. *Physical Chemistry Chemical Physics*[J], 2024, 26: 27602
7 Ali I H, Sharifi R, Javidparvar A A *et al. Journal of Industrial and Engineering Chemistry*[J], 2025, 150: 719
8 Zhang X, Guo R, Feng X *et al. Processes*[J], 2024, 12: 2408
9 Wang G, Wang H, Cui Q *et al. Metals*[J], 2023, 13: 322
10 Xavier J R, Vinodhini S P, Ganesan R. *Journal of Materials*

Science[J], 2024, 59: 12830
11 Sun R, Liu P, Qi H *et al. Journal of Nanoparticle Research*[J], 2019, 21: 72
12 Liu P, Sui P, Feng Z *et al. Journal of Nanoparticle Research*[J], 2020, 22: 240
13 Liu Y, Li A, Lei Y *et al. Scientific Reports*[J], 2025, 15: 8287
14 Guo J, Sun R, Qi H *et al. Coatings*[J], 2019, 9: 557
15 Fan X, Pan D, Li M. *Acta Materialia*[J], 2020, 193: 280
16 Ju Y, Zhang Q, Gong Z *et al. Journal of Applied Physics*[J], 2013, 114: 093507
17 Cui G, Bi Z, Zhang R *et al. Chemical Engineering Journal*[J], 2019, 373: 104
18 Hwang J, Tak W S, Mun S Y *et al. Materials*[J], 2020, 13: 3602
19 Pradhan S K, Sahoo M R, Ratha S *et al. AIP Advances*[J], 2020, 10: 065016
20 Creighton M A, Yuen M C, Morrisac N J *et al. Nanoscale*[J], 2020, 12: 23995
21 Liu P, Liu J, Wang M. *Combustion and Flame*[J], 2019, 201: 276
22 Fedorov A V, Shulgin A V, Lavruk S A. *Combustion, Explosion, and Shock Waves*[J], 2016, 52: 457
23 Levitas V I, Pantoya M L, Chauhan G *et al. The Journal of Physical Chemistry C*[J], 2009, 113: 14088
24 Sun R C, Jia C Y, Mi G B. The mechanism of the influence of Mo content on the flame-retardant properties of titanium alloys[J/OL]. *Transactions of Nonferrous Metals Society of China*, 2026-06-09. https://link.cnki.net/urlid/43.1239.TG.20260608.1656.004
25 Yang C C, Mai Y W. *Materials Science and Engineering R*[J], 2014, 79: 1
26 Shu Q, Yang Y, Zhai Y T *et al. Nanoscale*[J], 2012, 4: 6307
27 Alavi S, Thompson D L. *Journal of Physical Chemistry A*[J], 2005, 110: 1518
28 Sun J, Simon S L. *Thermochimica Acta*[J], 2007, 463: 32
29 Liu J, Wang M, Liu P. *Materials Research Express*[J], 2018, 5: 065011
30 Gao Y, Zhu W, Wang T *et al. The Journal of Physical Chemistry C*[J], 2022, 126: 11058
31 Hong S, van Duin A C. *The Journal of Physical Chemistry C*[J], 2015, 119: 17876
32 Sun R, Liu P, Qi H *et al. Materials Research Express*[J], 2020, 6: 1250
33 Sun R, Mi G, Huang X *et al. Modern Physics Letters B*[J], 2024, 38: 2350263
34 Sun R, Mi G. *Rare Metal Materials and Engineering*[J], 2024, 5(3): 2405
35 Chu Y, Wang L, Liu P *et al. ACS Omega*[J], 2023, 8: 32712
36 Thompson A P, Aktulga H M, Berger R *et al. Computer Physics Communications*[J], 2022, 271: 108171
37 Plummer G, Rathod H, Srivastava A *et al. Materials Today*[J], 2021, 43: 45
38 Plummer G, Tucker G J. *Physical Review B*[J], 2019, 100: 214114
39 Stukowski A. *Modelling and Simulation in Materials Science and Engineering*[J], 2009, 18: 015012
40 Hong S, van Duin A C. *The Journal of Physical Chemistry C*[J], 2016, 120: 9464
41 Wu Chenglin, Dong Shiyun, Yan Shixing *et al. Rare Metal Materials and Engineering*[J], 2025, 54(10): 2684 (in Chinese)

连续热能输入条件下铝基碳包覆纳米核壳复合颗粒的分子动力学模拟

刘洪波[1]，李奥杰[2]，马文江[3]，陈章华[1]，刘　一[2]
（1. 北京科技大学 数理学院，北京 100083）
（2. 昆明理工大学 建筑工程学院，云南 昆明 650031）
（3. 北京科技大学 自然科学基础实验中心，北京 100083）

摘　要：纳米铝粉（ANP）是典型金属燃料推进剂，通过在ANP表面形成碳包覆层，构建出一种新型纳米核壳复合颗粒。在作为金属基推进剂燃料的应用中，这种纳米核壳复合颗粒在点火和燃烧前会快速吸收热能，从而实现点火和燃烧。采用分子动力学模拟揭示纳米复合颗粒在加热过程中的组织演化机制，并分析核壳界面的迁移过程。结果表明，粒径8 nm的碳包覆ANP复合颗粒的临界温度（材料从固态转变为液态的温度）约为1050 K。纳米复合颗粒的原子间势能低于铝芯。因此，在热能注入下，初始的非晶相转变为液相，随后液相从表面向核心扩散。较低的原子间势能导致非晶相较早转变为液相。此外，核壳比是影响临界熔点的主要因素。核壳比越高，即碳涂层越薄，熔点越低。因此有效控制该参数是决定点火效能的重要因素。

关键词：分子动力学；碳包覆层；ANP；纳米核壳复合颗粒

作者简介：刘洪波，男，1980年生，博士生，北京科技大学数理学院，北京 100083，E-mail：b20200377@xs.ustb.edu.cn